JEAS

JOURNAL OF ENGINEERING AND APPLIED SCIENCES

Journal of Engineering and Applied Sciences 13 (2018), 63-82

KINETICS AND MECHANISMS OF NITRIC ACID LEACHING OF ALUMINA FROM AMAGUNZE CLAY

Ikechukwu A. Nnanwube[1*], Okechukwu D. Onukwuli[2]
[1,2]Department of Chemical Engineering, NnamdiAzikiwe University, Awka
[*]CorrespondingAuthor's E-mail: ik.nnanwube@gmail.com

Abstract
This study was concerned with the physicochemical characterization and kinetics study of Amagunze clay dissolution in nitric acid. The effects of acid concentration, temperature, particle size, stirring speed and solid/liquid ratio on the leaching of alumina from Amagunze clay were investigated. The X-ray fluorescence data revealed the presence of Al_2O_3 and SiO_2 as major oxides. Metals such as Mg, K, Ca, andTi exist as minor elements while Cr, Zn, Mn and Sr exist as traces. The analysis of Amagunze clay by X-ray diffraction revealed the presence of microline and quartz. The FTIR result confirmed the results of XRF and XRD analysis by revealing the presence of relevant functional groups. Results of the leaching studies showed that alumina dissolution in nitric acid increased with increasing concentration of nitric acid, temperature and stirring rate, and decreased with increasing particle diameter and solid/liquid ratio. In 10M HNO_3, at a temperature of 363K using 75µm particle diameter with solid/liquid ratio of 20g/L and stirring speed of 540 rpm, about 85.4% of alumina dissolved in 150 minutes. The activation energy, reaction order and Arrhenius constant calculated at the conditions above were 15.36 KJ/mol, 0.41, 0.586 s^{-1}, respectively. The mechanism of dissolution of alumina was established to follow the shrinking core model for the surface chemical reaction mechanism. The XRD analysis of the post-leaching residue revealed the presence of microline and quartz. Hence, Amagunze clay has proved to be a viable alternative source for alumina production.

Keywords: Alumina, Amagunze clay, Leaching, Kinetics, Nitric acid.

1. Introduction

Alumina is a white powder produced normally from bauxite ore through alkali leaching by the Bayer process. It is commercially important and a major raw material for the production of aluminium metal. More than 90% of the world's commercial production of alumina is obtained by hydrochemical sodium hydroxide extraction of bauxite using the conventional Bayer process. In this process it is uneconomical to treat bauxite containing more than 7% reactive silica, due to excessive alumina and soda losses (Connor, 1988). Such quality of bauxite deposits are fairly rare and most of those available being controlled by world's largest aluminium manufacturing concerns. Intensive research and engineering effort has been carried out in many countries on the alumina extraction from a variety of naturally occurring non-bauxitic materials such as laterites, clay, aluminous shales, nepheline, alunite and fly ash. A range of acid and alkali hydrometallurgical processes have been proposed as routes for extraction of alumina. Acid rather than alkali processes are preferred for aluminium silicates and especially for processing of koalinitic material (Al-Ajeel and Al-Sindy, 2006).

Clay is a naturally occurring aluminium silicate composed of fine-grained minerals. The clay mineral is composed essentially of silica, alumina or magnesia or both, and water, but iron substitutes for aluminium and magnesium in varying degrees, and appreciable quantities of potassium, sodium, and calcium are frequently present as well. These

essential elements of the clay mineral can be leached out by treating the clay with mineral acid solution (Ajemba and Onukwuli, 2012).

Clay dissolution in acid medium is gaining serious academic attention in the recent time. This is as a result of the need of a low cost source of metallic ores (Ajemba and Onukwulli, 2012). Acid treatment of clay mineral is one of the most common chemical modifications of clays, used for both industrial and scientific purposes. Prior to acid treatment, the clay mineral is usually calcined to increase its dissolubility in the acid solution (Brown and Hrishikesan, 1962). Calcination is a thermal treatment process applied to ores and other solid materials to bring about a thermal decomposition, phase transition, or removal of a volatile fraction (Ajemba and Onukwuli, 2012).

As bauxite ores continue to deplete, there is need for alternative local source of alumina for aluminium industries in Nigeria. Amagunze clay which contains a high amount of alumina is a readily available alternative. To the best of our knowledge, no work has been published on the recovery of alumina from Amagunze clay. This work will therefore, serve as a good reference material on alumina recovery from Nigerian clays via nitric acid route.

2.0 Material and methods

2.1 Materials

2.1.1 Sample mining and preparation

The clay used for this study was collected from Amagunze, Nkanu-east L. G. A, Enugu State of Nigeria. The clay samples were sun-dried for 48 hours and oven-dried at 60^{o}C for 72 hours. The clay was finely pulverized and sieved into five fractions: 75, 106, 212, 300, and 425 µm. The sieved clay samples were then calcined in a muffle furnace at a temperature range of 400^{o}C – 800^{o}C. All experiments were performed with 75 µm fraction except otherwise stated. Solutions of HNO_3 were prepared from analytical grade reagents with deionized water.

2.2 Characterization of the clay

2.2.1 Spectrophotometric analysis

The X-ray fluorometer (XRF), X-supreme 600 oxford instrument, was used for the elemental analysis of the clay. The mineralogical analysis of the clay was done using ARL X'TRA X-ray Diffractometer, Thermoscientific with the serial number 197492086 and Empyrean by PanAnalytical model with CuKα (1.54 Å) radiation generated and 40mA and 45kV. This unit comprises of a single compact cabinet. The cabinet houses a high speed, high precision Goniometer; high efficiency generator (X-ray) and an automatic sample loading facility.

The petrographic slides of the clay were prepared using Epoxy and Lakeside 70 media according to the method of Hutchison (Hutcison, 1974).

2.2.2 FTIR and SEM analysis

FTIR analysis was carried out using Buck Scientific M530 Infrared Spectrophotometer. SEM analysis was carried out using Q250 by FEI model from the Netherlands.

2.3 Leaching procedure

Leaching experiments were performed in a 500 ml glass reactor fitted with a condenser to prevent losses through evaporation. The two major variables (heat and stirring rate) necessary for accelerating the rate of chemical reaction was provided by the aid of a magnetically-stirred hot plate (Model 78HW-1). For every leaching experiment, the solution mixture was freshly prepared by dissolving 20 g/L of the clay sample in the acid solution at 363 K. The concentration which gave the maximum dissolution was subsequently used to study other leaching parameters including temperature and particle size. At the end of each reaction time, the undissolved materials in the suspension

was allowed to settle and separated by filtration. The resulting solutions were diluted and analyzed for alumina using atomic absorption spectrophotometer (AAS).

The mole fraction of alumina passing into the solution from the calcined clay was calculated by the formula given in Equation (1), where *x* designates quantity dissolution.

$$x = \frac{\text{Amountof } Al^{3+} \text{ that passedintothesolution}}{\text{Amountof } Al^{3+} \text{inoriginalsample}} \quad (1)$$

The activation energy, E_a , and rate constants were evaluated from the Arrhenius plots. The post-leached residues after dissolution in the optimum conditions were subjected to XRD and SEM examination.

3.0 Results and Discussions

3.1 XRF analysis of Amagunze clay

The results of the elemental composition of Amagunze clay by X-ray fluorescence technique showed that the clay exist mainly as aluminosilicate with some quantities of Fe. Metals such as Mg, K, Ca, andTi exist as minor elements while Cr, Zn, Mn and Sr exist as traces. The elemental analysis is summarized in Table 1.

Table 1: XRF results of Amagunze clay

Chemical constituent	Wt(%)
MgO	1.155
Al_2O_3	27.253
SiO_2	53.985
P_2O_5	0.135
SO_3	0.198
Cl	0.003
K_2O	3.614
CaO	0.618
TiO_2	1.380
Cr_2O_3	0.017
Mn_2O_3	0.022
Fe_2O_3	11..557
ZnO	0.005
SrO	0.059

3.1.2 XRD analysis of Amagunze clay

The analysis of Amagunze clay by X-ray diffraction shows that the clay exists mainly as potassium aluminium silicate (microline). Table 2 present the results of the X-ray diffractogram of the clay with important compounds identified.

The clay gave two principal and one minor peaks at 3.34, 3.25, and 4.21 Å, respectively. The result reveals the presence of microline ($KAlSi_3O_8$) and quartz (SiO_2). All these supported the results of the elemental analysis by XRF.

Table 2: The X-ray diffraction data of the Amagunze clay showing the angle 2θ and d-values of the compounds identified, with their relative intensity (%).

2θ	d-Value (Å)	Compound	Intensity (%)	JCPDS file No.
20.86	4.25	Quartz (SiO_2)	21.62	01-087-2096
21.07	4.21	Microline ($KAlSi_3O_8$)	51.00	00-022-0687
25.68	3.47	Microline ($KAlSi_3O_8$)	26.00	00-022-0687
26.44	3.37	Microline ($KAlSi_3O_8$)	41.00	00-022-0687
26.64	3.34	Quartz (SiO_2)	100.00	01-087-2096
27.11	3.29	Microline ($KAlSi_3O_8$)	48.00	00-022-0687
27.45	3.25	Microline ($KAlSi_3O_8$)	100.00	00-022-0687
36.55	2.46	Quartz (SiO_2)	6.01	01-087-2096
39.47	2.28	Quartz (SiO_2)	5.91	01-087-2096

JCPDS file No. : Joint Committee on Power Diffraction Standards File Number

3.1.3 FTIR analysis of Amagunze clay

The Fourier Transform Infrared (FTIR) spectra of Amagunze clay is shown in Figure 1. The bands at 3761 cm^{-1}, 3397 cm^{-1}, 3227 cm^{-1}, 3107 cm^{-1}, 2982 cm^{-1}, 2900 cm^{-1}, 2750 cm^{-1}, and 2603 cm^{-1} are attributed to O-H stretching. The bands at 3107 cm^{-1} and 2450 cm^{-1} are attributed to N-H stretching while the band at 1634 cm^{-1} is attributed to N-H bending. The band at 859 cm^{-1} is attributed to Si-C stretching while the band at 1634 cm^{-1} is also attributed to Al-O-H stretching.

The FTIR result is in agreement with the XRF and XRD studies which confirmed the presence of the minerals detected.

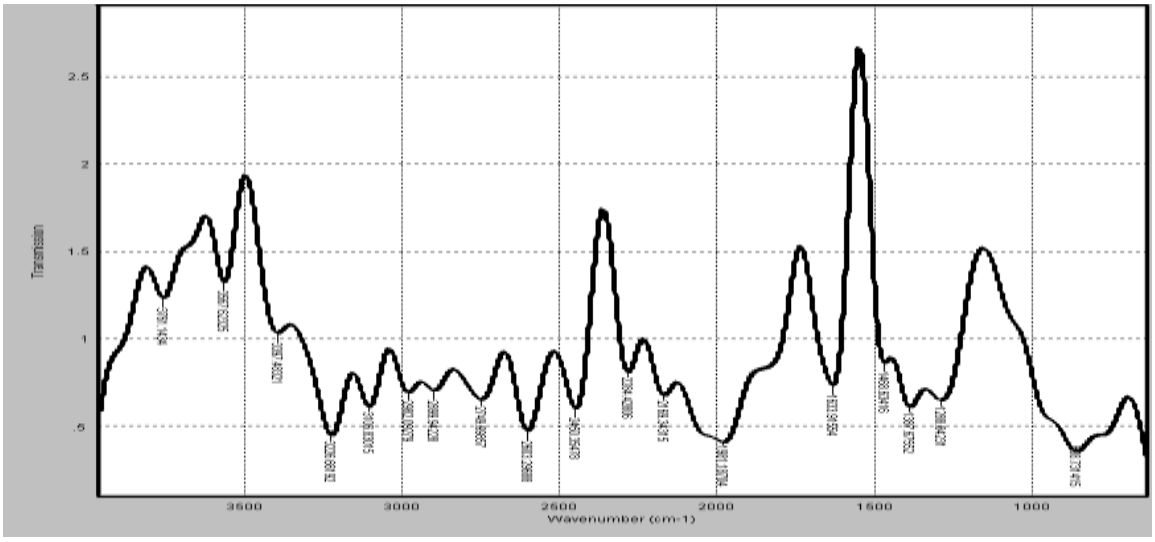

Figure 1: FTIR spectrum of Amagunze clay

3.1.4 SEM analysis of Amagunze clay

The scanning electron micrograph (SEM) of Amagunze clay was obtained with magnifications of 300x, 520x, 1500x, respectively as shown in Figure 2. The average cell diameter of the clay ranges from 34 to 113 µm while the average cell density ranges from 0.031 to 0.046 cell/mm. The results indicate that the clay particles are very cohesive, confirming their micrometer sized agglomerates composed of individual lamellae with rough edges and form microscopic flakes (Sthay and Ramaswamy, 2002). The clay may be poorly crystalline due to the presence of impurities. Several authors have found that impurity in elements and also illite decrease the whiteness of kaolinites (Schroeder et al., 2003; Divacaran and Sivasankara, 2004; Raghavan et al., 2004).

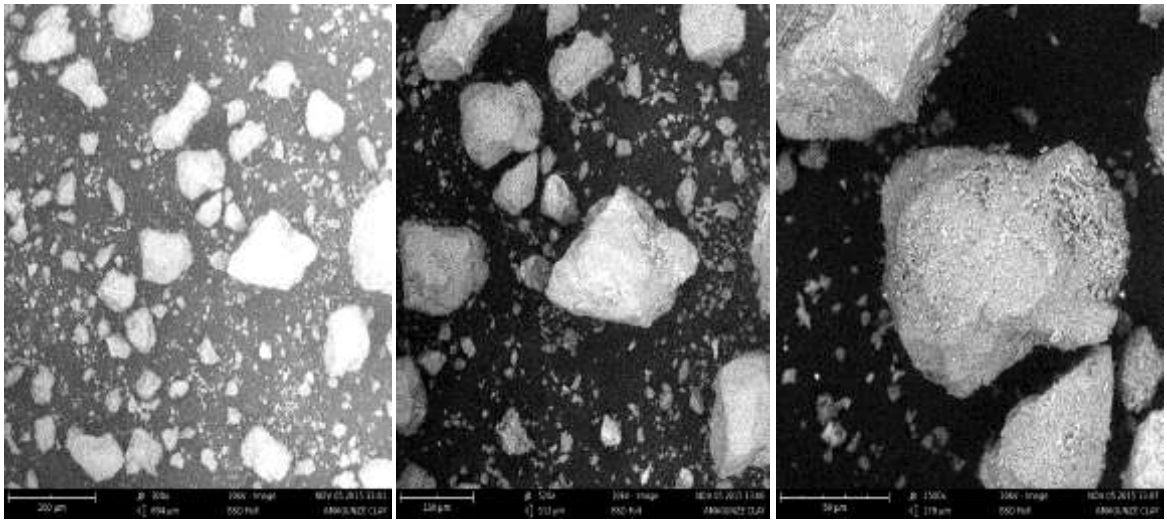

(a) (b) (c)

Figure 2: SEM image of Amagunze clay showing magnifications of 300× (a), 520× (b) and 1500× (c) respectively.

3.1.5 Effect of calcination temperature on alumina dissolution

The results of the effect of calcination temperature on alumina dissolution are shown in Figure 3. The results show that maximum dissolution rate of 74.9% was attained with a calcination temperature of 973 K in 150 minutes at the given conditions. Hence, a calcination temperature of 973 K was used for subsequent studies.

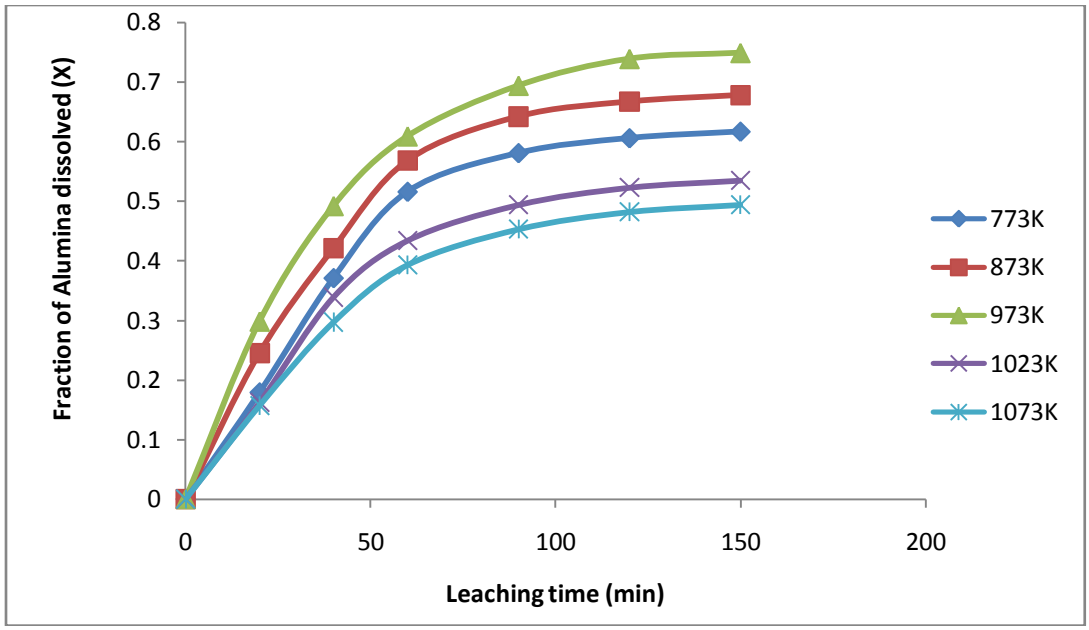

Figure 3: Effect of calcination temperature on alumina dissolution at various leaching time. *Experimental conditions:* particle size = 75 µm; solid/liquid ratio = 20 g/L; leaching temperature = 353K; stirring speed = 540 rpm; HNO_3 concentration = 6 M; calcinations time =1hour.

3.1.6 XRF analysis of Amagunze clay calcined at 973K

The results of the elemental composition of Amagunze clay by X-ray fluorescence technique showed that the clay exist mainly as aluminosilicate with some quantities of Fe. Metals such as Mg, K, Ca, and Ti exist as minor elements while Cr, Zn, Mn and Sr exist as traces. The result revealed that calcination caused some alterations in the chemical composition of the clay. From the results obtained, the percentage of aluminosilicate increased from 81.238wt% for the raw sample to 84.234wt % for the calcined sample. Hence, calcination helped to further purify the clay. The elemental analysis is summarized in Table 3.

Table 3: XRF results of Amagunze clay calcined at 973K

Chemical constituent	Wt (%)
MgO	1.0713
Al_2O_3	25.7471
SiO_2	58.487
P_2O_5	0.0709
SO_3	0.2395
Cl	0.0187
K_2O	3.629
CaO	2.3513
TiO_2	1.0621

Cr_2O_3	0.0103
Mn_2O_3	0.0294
Fe_2O_3	7.2293
ZnO	0.0103
SrO	0.0438

3.2. Leaching studies

3.2.1 Effect of HNO_3 concentration on alumina dissolution

The results of the effect of HNO_3 concentration on alumina dissolution are illustrated in Figure 4. The results show that the fraction of alumina dissolved increased with increase in acid concentration. The result obtained with 12 M HNO_3 was slightly lower than that obtained with 10 M HNO_3, and this could be attributed to the destruction of the clay structure by excess acid (Ajemba and Onukwuli, 2012).

In all cases, unreacted acid remained in the leach solution and the free acid increased with increasing initial acid concentration, since the use of more concentrated acid did not increase the dissolution of alumina or decrease the leaching time for maximum dissolution. Therefore, 10 M HNO_3 was used for further investigation.

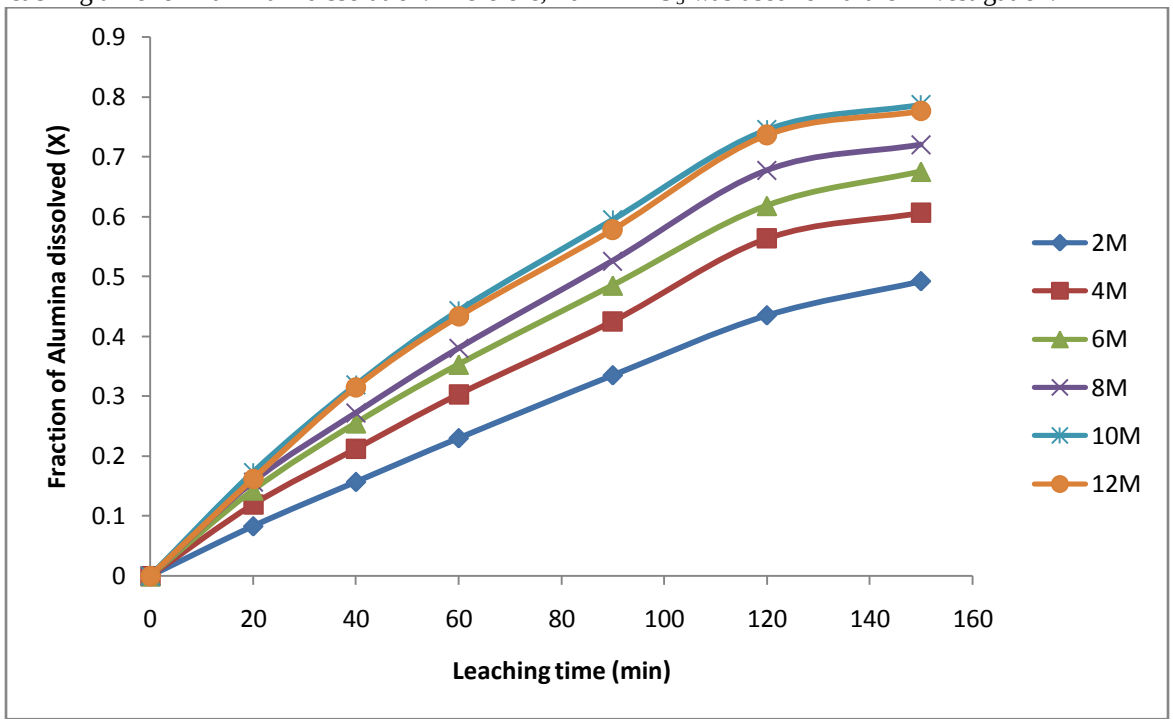

Figure 4: Effect of HNO_3 concentration on alumina dissolution at various leaching time. *Experimental conditions:* particle size = 75 µm; solid/liquid ratio = 20 g/L; leaching temperature = 363K; stirring speed = 540 rpm; calcination temperature = 973K.

3.2.2 Effect of stirring rate on alumina dissolution

The results on the effect of stirring rate on alumina dissolution in 10M HNO_3 over the range of 90-720 rpm at 363K is presented in Figure 5.

Figure 5 shows that the amount of alumina dissolved is dependent on the stirring speed over the range 90-540 rpm. Above 540 rpm, the stirring speed no longer had any observable effect on alumina dissolution. Hence dissolution reached a steady rate at 540 rpm, and a stirring speed of 540 rpm was retained for further experiments. Increase in stirring rate causes a decrease in the thickness of the film layer, therefore, causing an increase in the dissolution rate (Ajemba and Onukwuli, 2012).

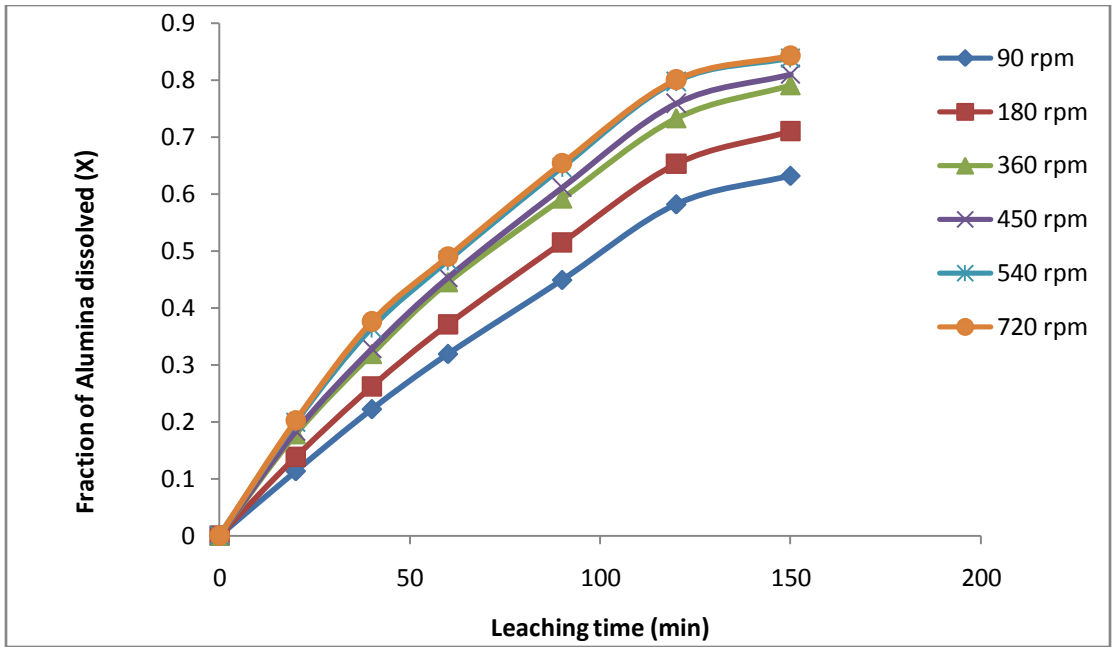

Figure 5: Effect of stirring rate on alumina dissolution at various leaching time. *Experimental conditions:* particle size = 75 µm; solid/liquid ratio = 20 g/L; leaching temperature = 363K; HNO_3 concentration = 10M; calcination temperature = 973K.

3.2.3 Effect of leaching temperature on alumina dissolution

The effect of temperature on alumina dissolution has been investigated over the temperature range 303-363 K in 10 M HNO_3 solution at a stirring rate of 540 rpm using 75 µm particle diameter and solid/liquid ratio of 20 g/L. These results are presented in Figure 6.

As seen in Figure 6, alumina dissolution increased with increase in temperature. This is as a result of high kinetic energy available for the reacting molecules (Ajemba and Onukwuli, 2012). At 373K, the amount of alumina dissolved within 150 min was 86.8%.

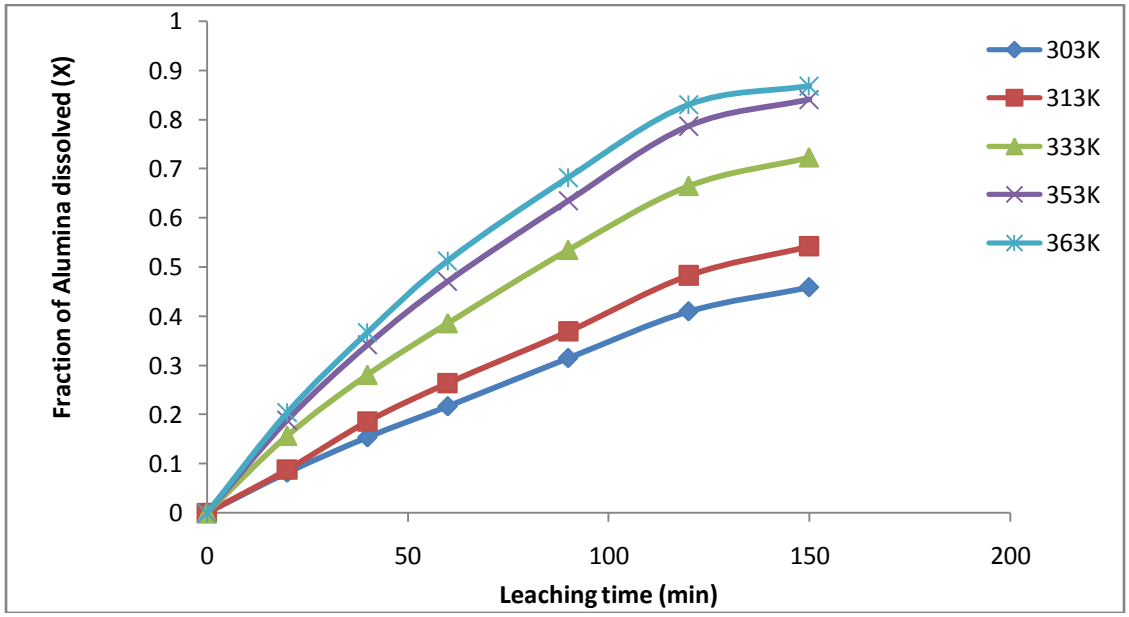

Figure 6: Fraction of alumina dissolved vs. leaching time at different temperatures. *Experimental conditions:* particle size = 75 µm; solid/liquid ratio = 20 g/L; stirring rate = 540 rpm; HNO_3 concentration = 10M; calcination temperature = 973K.

3.2.4 Effect of solid/liquid ratio on alumina dissolution

The results on the effect of solid/liquid ratio on alumina dissolution in 10 M HNO_3 were investigated in the range 0.02 to 0.045 g/ml at a temperature of 363K. Figure 7 shows the effect of solid/liquid ratio on alumina dissolution in 10 M HNO_3. Decreasing the solid/liquid ratio was accompanied with increase in the equilibrium percentage of alumina dissolved. For instance, by varying the solid/liquid ratio from 0.045 to 0.02 g/ml, the percentage of alumina dissolved increased from 58.5% to 88.5% at 363 K. This could be attributed to the decrease in the fluid reactant per unit weight of the solid (Ajemba and Onukwuli, 2012). Accordingly, an optimum solid/liquid ratio 0.02 g/ml was retained for subsequent studies.

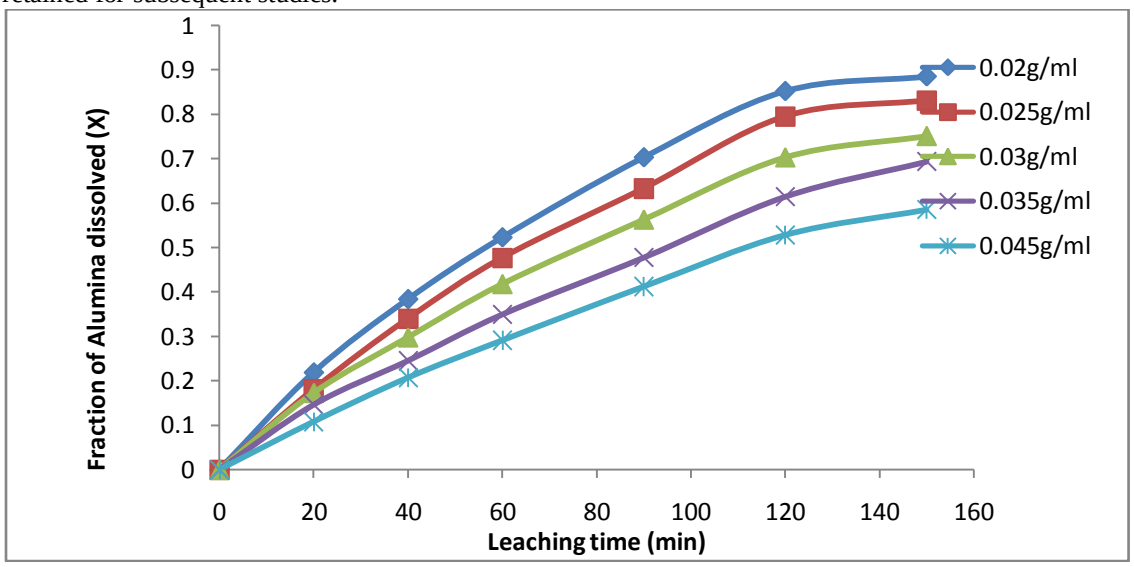

Figure 7: Effect of solid/liquid ratio on alumina dissolution. ***Experimental conditions:*** **HNO_3 concentration = 10 M; particle diameter = 75 µm; stirring rate = 540 rpm; leaching temperature = 363K; calcination temperature = 973K.**

3.2.5 Effect of particle size on alumina dissolution

The influence of particle diameter on alumina dissolution in HNO_3 was investigated for five different sized fractions. The results are summarized in Figure 8

The results from Figure 8 indicate that the dissolution rate is inversely proportional to the particle size. This is attributed to larger specific surface area provided by the smaller particles for contact with the acid molecules (Ajemba and onukwuli, 2012). This observation was also supported by Aydogan et al. (2007a) and (Dutrizac and MacDonald (1977)).

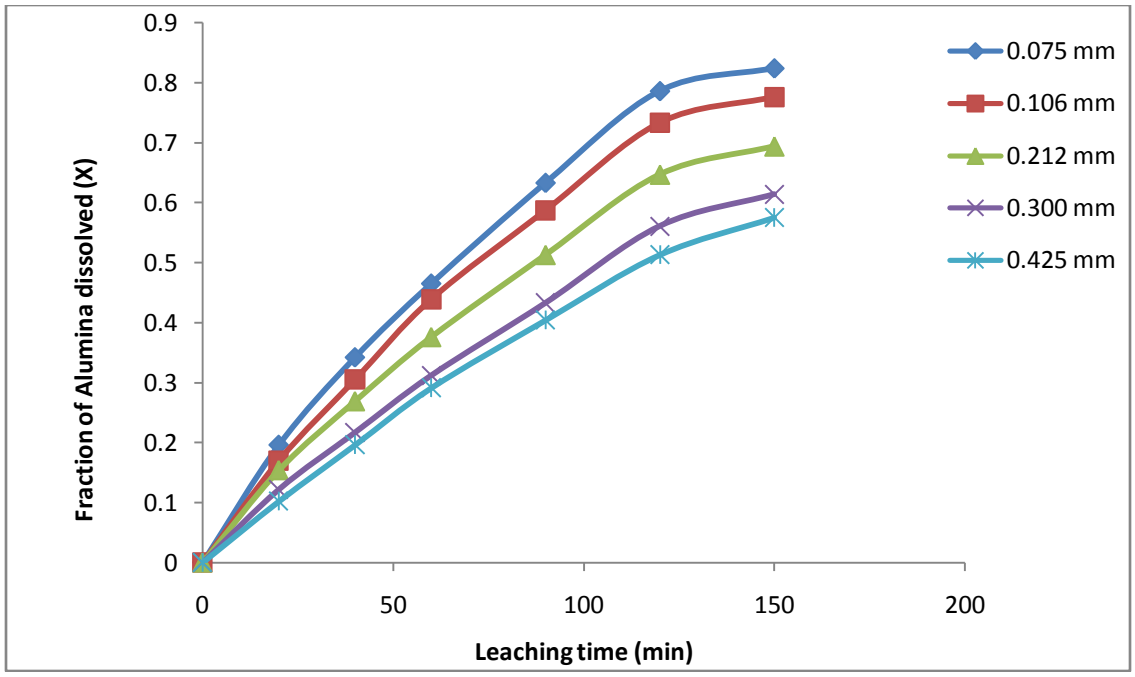

Figure 8: Effect of particle diameter on alumina dissolution. ***Experimental conditions:*** **HNO_3 concentration = 10 M; solid/liquid ratio = 20 g/L; stirring rate = 540 rpm; leaching temperature = 363K; calcination temperature = 973K.**

3.2.6 Dissolution kinetic models for the dissolution of Amagunze clay in nitric acid (HNO_3)

For this study, three shrinking core models were tested for better understanding of the dissolution of Amagunze clay in HNO_3 media. The kinetic models as previously utilized by some authors such as Aydogan et al. (2007a,b), Baba and Adekola (2010), Habashi (2005), Khalique et al. (2005), Leao (2007) and Merwe (2003) include:

$$1 - (1 - X)^{1/3} = \frac{b k_s C_A}{\rho_s r_o} t = k_2 t \quad (2)$$

where X is the fraction of alumina dissolved at time t, b the stoichiometric coefficient of the reagent in the leaching reaction, k_s the kinetic constant, C_A the concentration of the lixiviant, ρ_s the density of the solid, r_o the initial radius of the solid, and k_2 the rate constant from Equation (2).

$$1 + 2(1 - X) - 3(1 - X)^{2/3} = \frac{6 b D_e C_A}{\rho_s r_o^2} t = k_3 t \quad (3)$$

$$1 - (1 - X)^{1/3} + (y/6)\left[(1 - X)^{1/3} + 1 - 2(1 - X)^{2/3}\right] = k_4 t \quad (4)$$

where D_ϵ is the effective diffusion coefficient, k_3 and k_4 are the rate constants for Equations (3) and (4) respectively, y is taken to be 1 for heterogeneous systems.

Equation (2) is applicable to a chemical reaction controlled process at the interface; Equation (3) is a diffusion-controlled process through the product layer and Equation (4) is a mixed controlled process (a combination of surface reaction and diffusion). Of all the three models tested, all the studied data were found only to fit the relation in Equation (2) with a perfect correlation of about 0.99. The analysis of the plots of other kinetic curves, however, gave lower correlation coefficients. Hence, the linearization of Figures 4 – 8 was made. To this end, the relation: $1 - (1 - X)^{1/3} = k_1 t$, gave an average correlation coefficient of 0.993 and this is shown in Figure 9.

From Figure 9, the experimental rate constant k_1 , was calculated from the slope of the straight line at various HNO_3 concentrations and the plots of In k_1 versus In $[HNO_3]$ are shown in Figure 10.

From Figure 10 the slope of the resulting plot gave 0.41. This shows that the order of reaction with respect to H^+ ion concentration is 0.41 with correlation coefficient of 0.985.

Similarly, the apparent rate constant k_5 was calculated from the slope of the straight line at various stirring rates (w) as shown in Figure 11 and the plots of In k_5 versus In w are shown in Figure 12.

Furthermore, the data in Figure 6 at different temperatures were linearized by Equation (2). This is shown in Figure 13. The data in Figures 7 and 8 were also linearized by means of Equation (2) as shown in Figures 15 and 16, respectively.

From Figure 13, the apparent rate constants, k_2 and other tested constants, k_3 and k_4 were calculated from the slopes of the straight lines. The values of these rate constants with their equivalent correlation coefficients are summarized in Table 4.

Table 4: The values of rate constants k_2, k_3 and k_4 with their correlation coefficients for Amagunze clay dissolution at different temperatures by 10M HNO_3.

Temperature(K)	Apparent rate constants (10^{-3} min^{-1})			Correlation coefficient, R^2		
	K_2	K_3	K_4	K_2	K_3	K_4
303	1.29	0.53	1.87	0.996	0.911	0.994
313	1.58	0.78	2.27	0.997	0.909	0.995
333	2.44	1.68	3.42	0.994	0.928	0.989
353	3.18	2.65	4.36	0.995	0.923	0.991
363	3.47	3.05	4.73	0.991	0.931	0.986

By using the rate constants derived from the slopes in Figure 13, the Arrhenius diagram in Figure 14 was plotted from which the activation energy of 15.36KJ/mol was calculated. The Arrhenius constant for the process was estimated to be 0.586 s^{-1} with a correlation coefiicient of 0.990. In some instances and as reported by Olanipekun (1999), the rate controlling mechanism of the heterogeneous dissolution process could either be predicted from plots of the kinetic equations or from the activation energy.

In general and as demonstrated by Aydogan et al. (2007b), it has been accepted that a diffusion-controlled process is characterized by a slight dependence on temperature, while the chemically controlled process is strongly dependent on temperature. The reason being that diffusion coefficient, D, is linearly dependent on temperature formulated as: $k = A\ e^{-Ea/RT}$, where A is the Arrhenius constant, E_a is the activation energy, R is the Boltzmann constant and T is the absolute temperature.

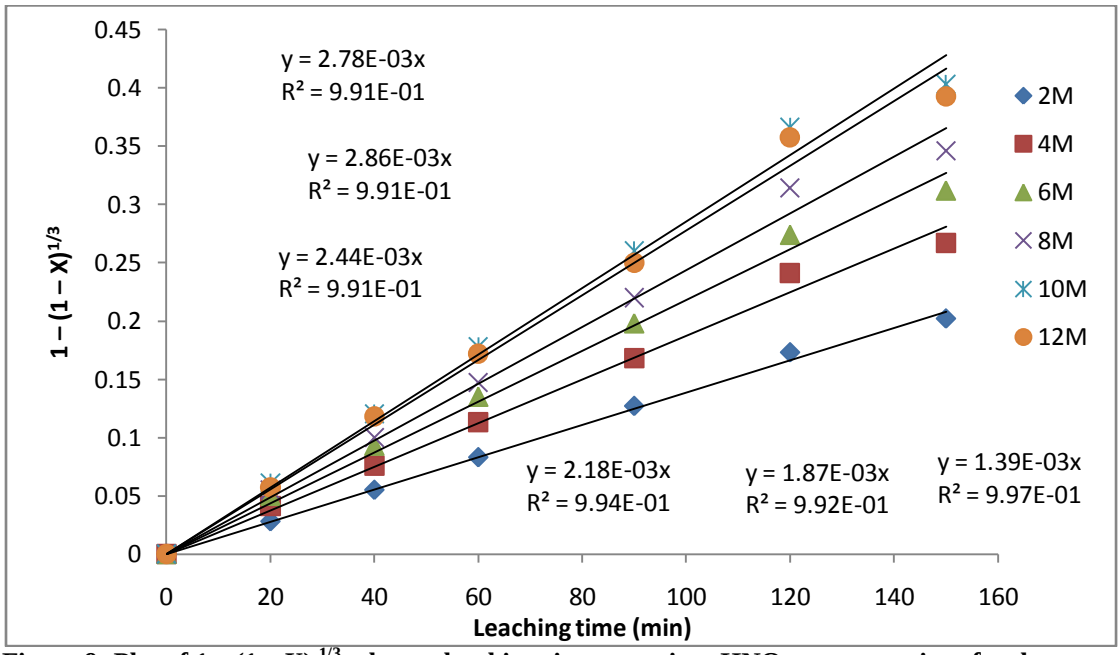

Figure 9: Plot of $1 – (1 – X)^{1/3} = k\ t$ vs. leaching time at various HNO_3 concentrations for data presented in Figure 4.

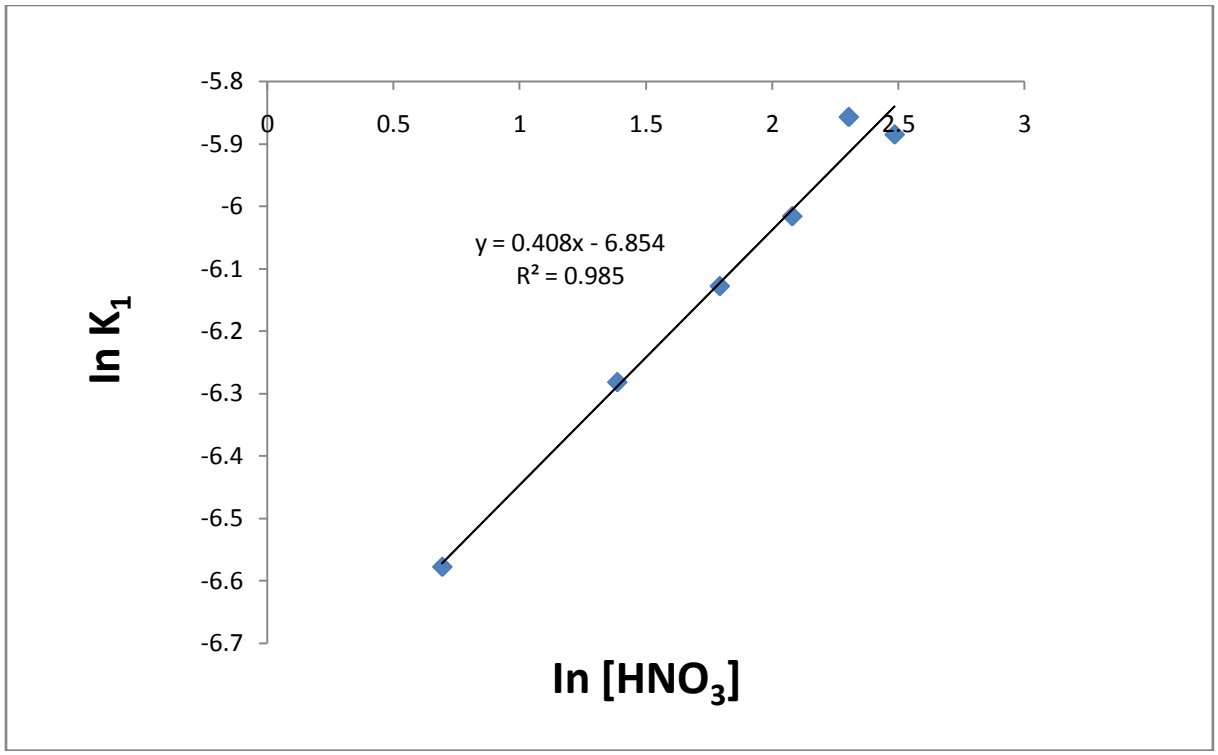

Figure 10: Plot of In k_1 vs. In [HNO_3], for determining order of acid concentration.

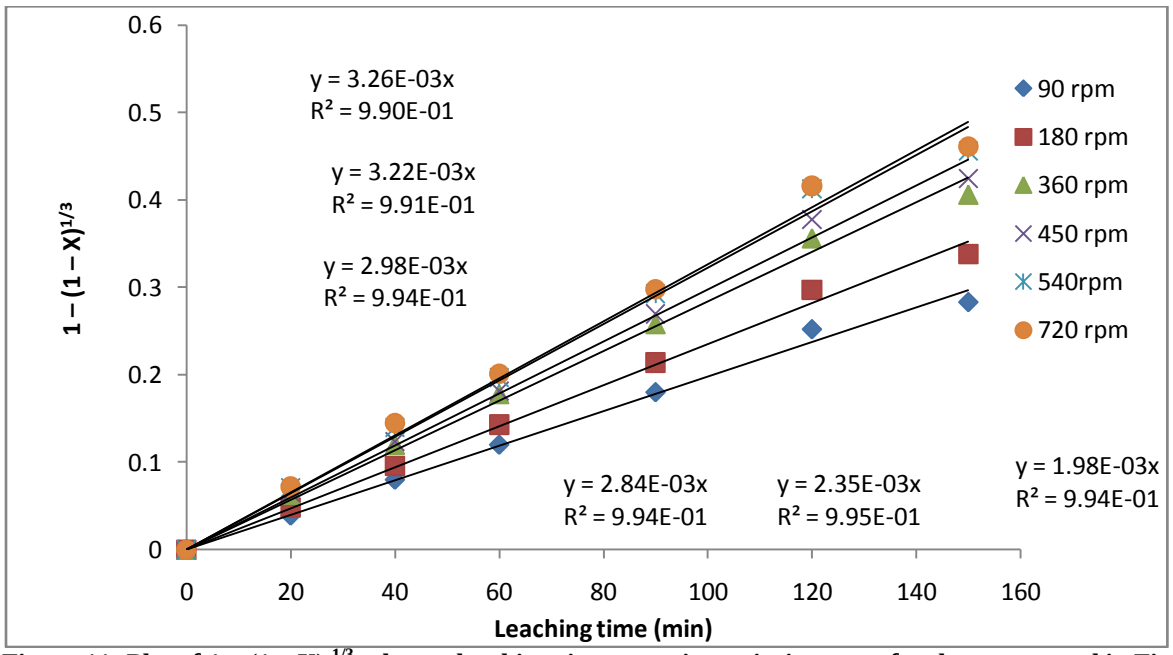

Figure 11: Plot of 1 – (1 – X) $^{1/3}$ = k t vs. leaching time at various stirring rates for data presented in Figure 5.

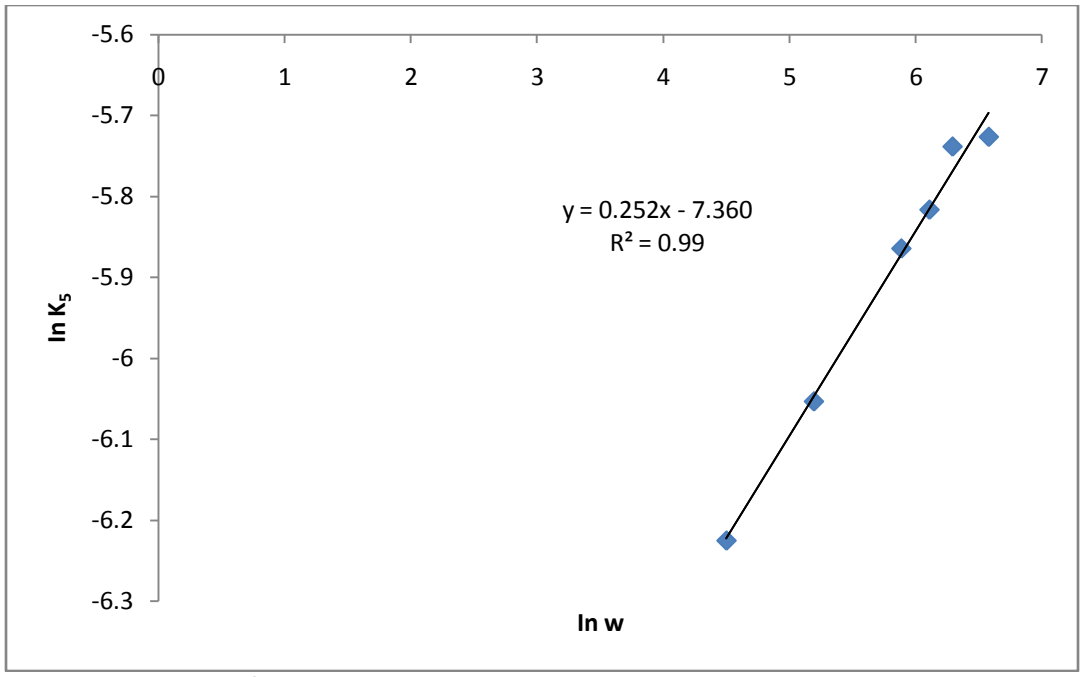

Figure 12: Plot of In k_5 vs. In w, for determining order of stirring rate.

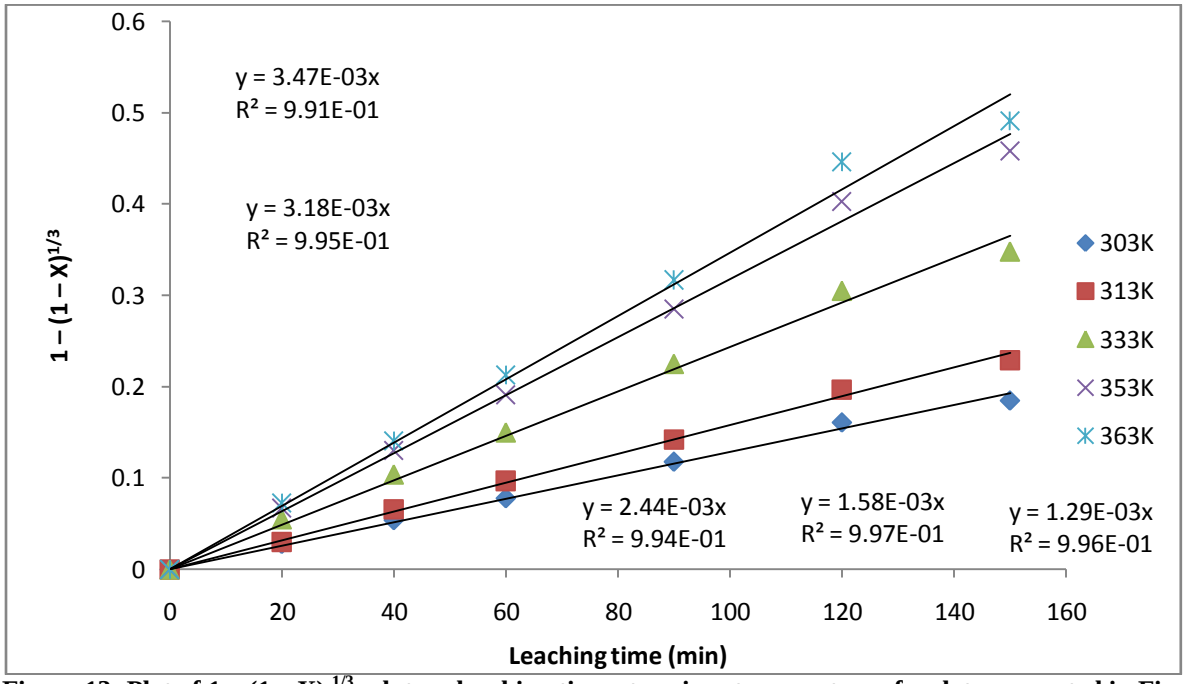

Figure 13: Plot of 1 – (1 – X) $^{1/3}$ = k t vs. leaching time at various temperatures for data presented in Figure 6.

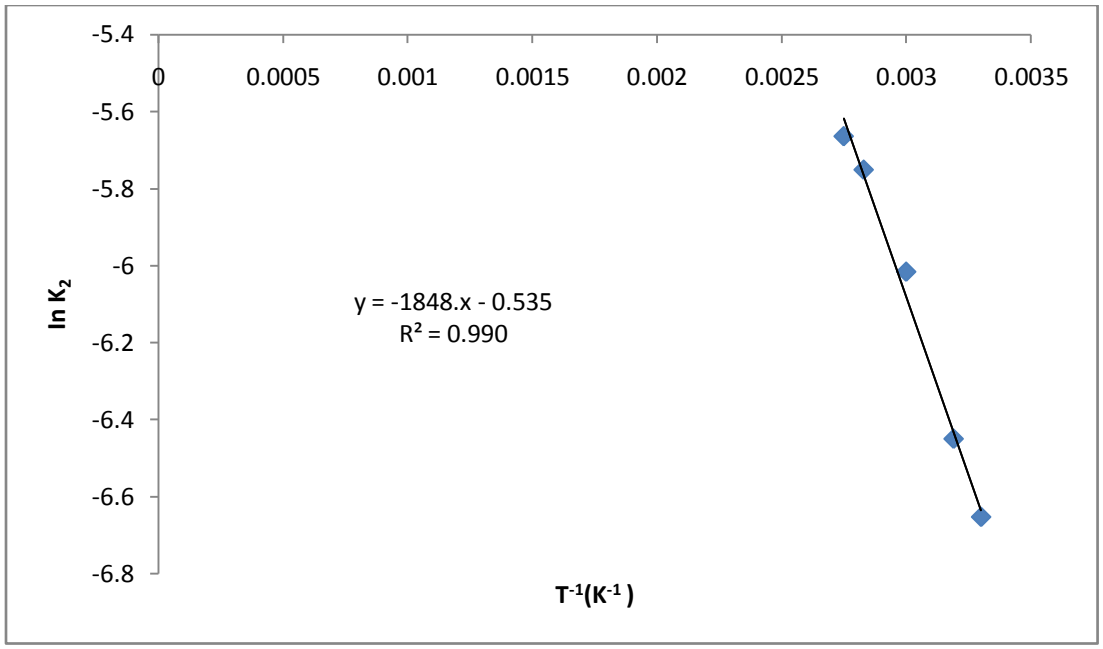

Figure 14: Arrhenius plot of reaction rate against reciprocal of temperature.

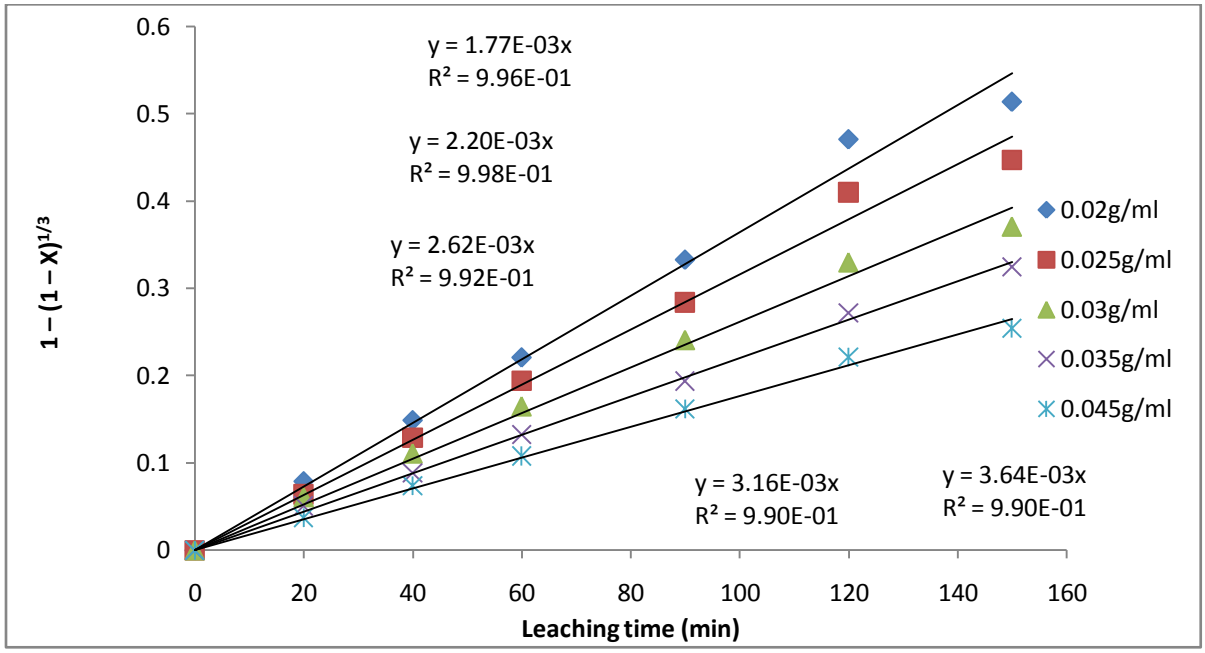

Figure 15: Plot of 1 – (1 – X) $^{1/3}$ = k t vs. leaching time at various solid/liquid ratios for data presented in Figure 7.

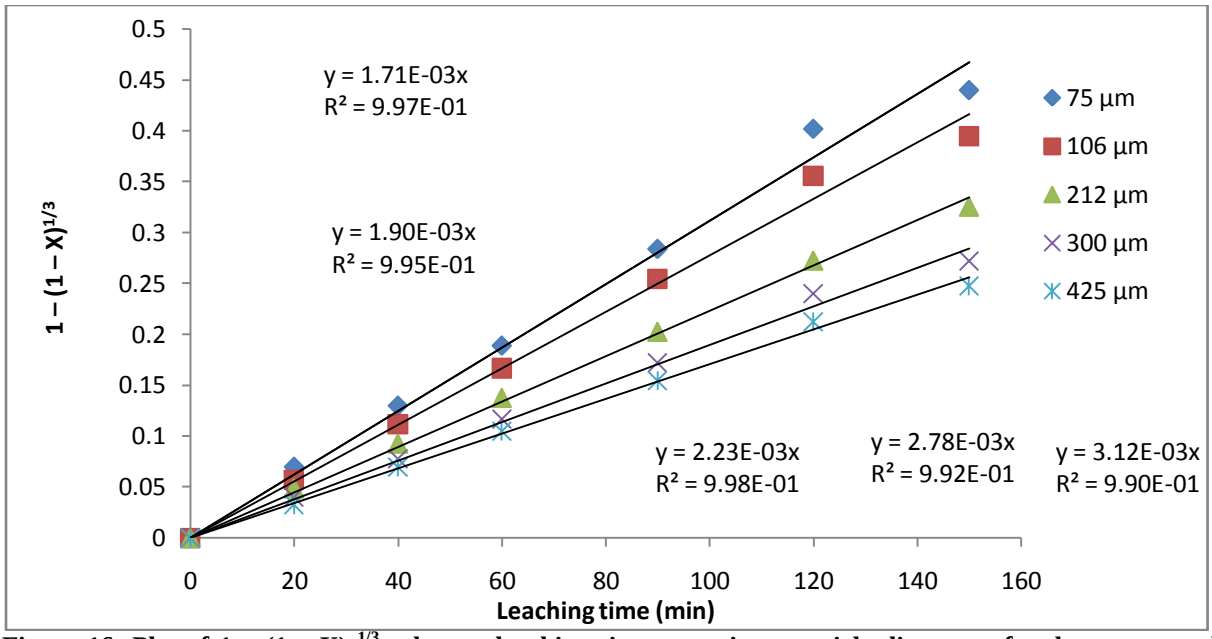

Figure 16: Plot of 1 – (1 – X) $^{1/3}$ = k t vs. leaching time at various particle diameters for data presented in Figure 8.

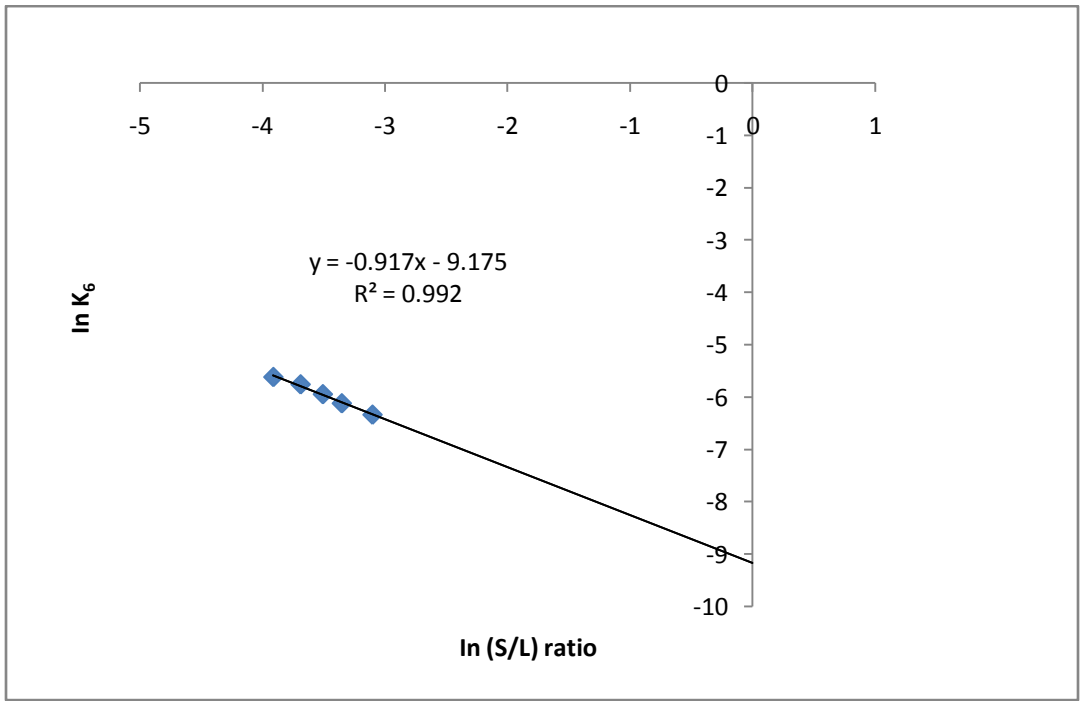

Figure 17: Plot of In k_6 vs. In (S/L), for determining order of solid/liquid ratio.

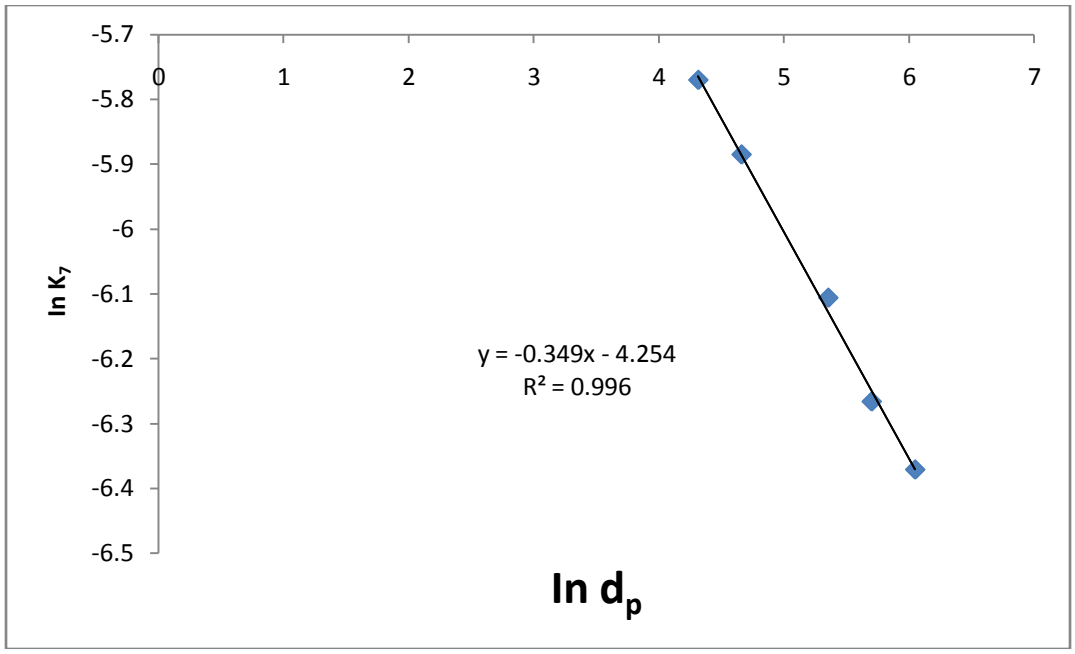

Figure 18: Plot of In k_7 vs. In d_p, for determining order of initial particle diameter.

3.2.7 Dissolution model

From the effects of the solid/liquid ratio (Figure 17) and particle diameters (Figure 18) on Amagunze clay dissolution in 10M HNO_3 solution, the apparent rate constants, k_6 and k_7 were evaluated, respectively.

The solid/liquid ratio and initial particle size (d_p) were found to be inversely proportional to 0.92 power $(S/L)^{-0.92}$ and 0.35 power ($d_p^{-0.35}$), respectively. Hence, the proposed model equation for Amagunze clay dissolution by 10M HNO_3 solution at 363 K is consistent with the following relation:

$$1 - (1 - X)^{1/3} = k_o C_{HNO_3}^{0.408} (d_p)^{-0.349} \left(\frac{S}{L}\right)^{-0.917} (w)^{0.252} e^{(-15364.3/RT)}\ t.$$

where k_o is a reaction constant, which can be determined from the fraction of alumina dissolved, X, at a given time, t. The parameter, X is determined experimentally. For instance, at 363K, the value of X = 0.854 (85.4% dissolution); k_o is calculated to be $0.05s^{-1}$. The value of k_o, however, is found to vary depending on the leaching systems/conditions (Aydogan et al., 2007a; Fuerstenau et al., 1986).

3.3 Characterization of the residual product

3.3.1 SEM analysis of Amagunze clay leached with 10 M HNO_3

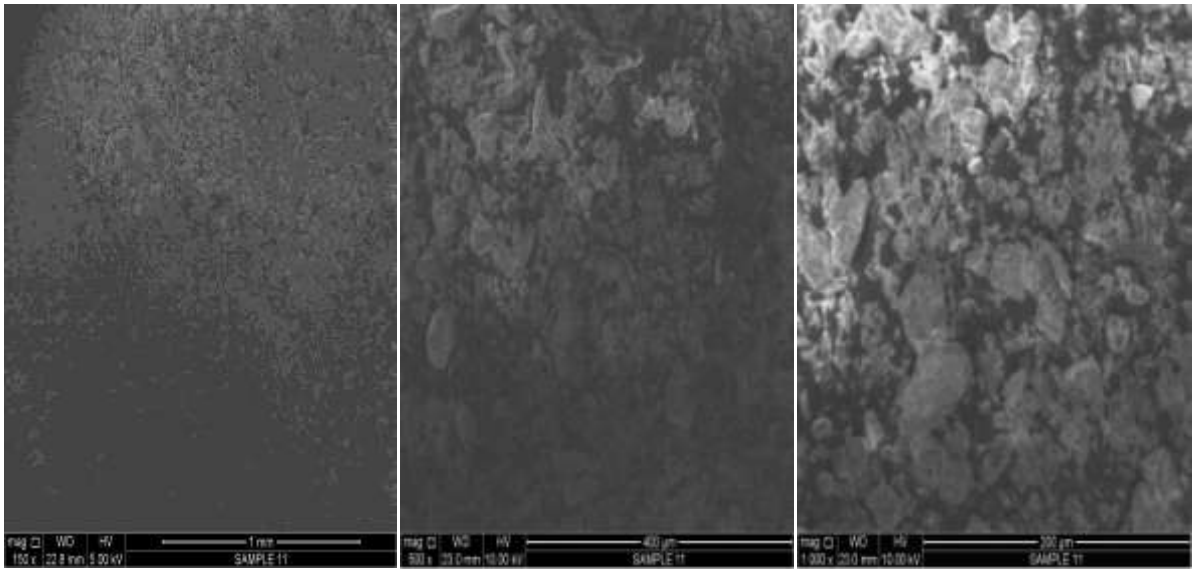

(a) (b) (C)

Figure 19: SEM image of Amagunze clay leached with 10M HNO_3 with magnifications of 150× (a), 500× (b), and 1000× (c) respectively.

The morphology of Amagunze clay after leaching with 10M HNO_3 solution was examined by scanning electron micrograph (SEM) and obtained with magnifications of 150×, 500× and 1000× respectively as shown in Figure 19. The average cell diameter ranges from 31 to 69μm while the average cell density ranges from 0.0854 to 0.148 cell/mm. The micrographs of the leaching residues show a progressive increase in the roughness of the solid (Souza et al., 2007). The particles have irregular shapes and form microscopic flakes.The particles may be poorly crystalline due to attack by the acid.

3.3.2 XRD analysis of Amagunze clay leached with 10 M HNO_3.

The analysis of Amagunze clay leached with 10M HNO_3 at 363K by X-ray diffraction gives a description of the mineral phases present in the residue. Table 5 present the results of the X-ray diffractogram of the residue. The XRD data revealed the presence of quartz and microline. The result showed one principal peak and two minor peaks at 3.34, 3.24, and 1.82 Å, respectively, as shown in Figure 20.

Table 5: The X-ray diffraction data of the Amagunze clay leached with 10M HNO_3 showing the angle 2θ and d-values of the compounds identified, with their relative intensity (%).

2θ	d-Value(Å)	Compound	Intensity (%)	JCPDS file No.
22.38	3.97	Microline ($K_{1.90}Na_{0.10}Al_2Si_6O_{16}$)	8.67	96-900-4192
23.27	3.82	Microline ($K_{1.90}Na_{0.10}Al_2Si_6O_{16}$)	4.81	96-900-4192
24.03	3.70	Microline ($K_{1.90}Na_{0.10}Al_2Si_6O_{16}$)	4.46	96-900-4192
25.66	3.47	Microline ($K_{1.90}Na_{0.10}Al_2Si_6O_{16}$)	9.85	96-900-4192
26.70	3.34	Quartz (Si_3O_6)	100.00	96-901-2601
27.50	3.24	Microline ($K_{1.90}Na_{0.10}Al_2Si_6O_{16}$)	35.22	96-900-4192

50.18	1.82	Quartz (Si_3O_6)	13.86	96-901-2601
		Microline ($K_{1.90}Na_{0.10}Al_2Si_6O_{16}$)		96-900-4192
50.61	1.80	Quartz (Si_3O_6)	6.66	96-901-2601
		Microline ($K_{1.90}Na_{0.10}Al_2Si_6O_{16}$)		96-900-4192

JCPDS File No. : Joint Committee on Power Diffraction Standards File Number.

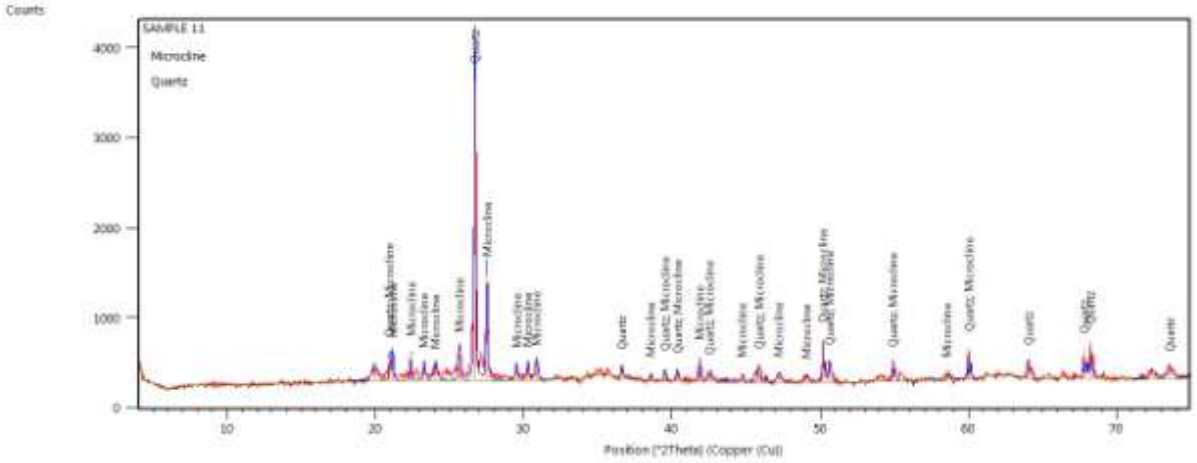

Figure 20: X-ray diffraction pattern of the post-leached residue of Amagunze clay after leaching for 150 minutes at 363K with 10M HNO_3.

4.0 Conclusion

Based on the results of the characterization and leaching investigations undertaken in this study, the following conclusions can be drawn:

i. The X-ray fluorescence data showed that Amagunze clay exist mainly as aluminium silicate with some quantities of Fe. Metals such as Mg, K, Ca, andTi exist as minor elements while Cr, Zn, Mn andSr exist as traces. The analysis of Amagunze clay by X-ray diffraction shows that the clay exists mainly as potassium aluminium silicate (microline). The XRD result reveals the presence of microline ($KAlSi_3O_8$) and quartz (SiO_2). The FTIR result was in agreement with the XRF and XRD studies as it confirmed the presence of the minerals detected. The SEM analysis revealed a low level of crystallinity.

ii. The leaching investigation clearly showed that alumina dissolution in nitric acid (HNO_3) increases with increasing concentration of nitric acid, temperature and stirring rate, and decreases with increasing particle diameter and solid/liquid ratio. In 10M HNO_3 at a temperature of 363K using 75µm particle diameter with solid/liquid ratio of 20 g/L and stirring speed of 540 rpm, about 85.4% of alumina was dissolved in 150 minutes. The values of activation energy, order of reaction and Arrhenius constant calculated at the conditions above for Amagunze clay were 15.36 KJ/mol, 0.41, 0.586 s^{-1}.

iii. The results of the dissolution studies indicated that the data fitted the shrinking core model for the surface chemical reaction mechanism. This is consistent with the following relation:

$$1-(1-X)^{1/3} = k_o C_{HNO_3}^{0.408} (d_p)^{-0.349} \left(\frac{S}{L}\right)^{-0.917} (w)^{0.252} e^{(-15364.3/RT)}\ t.$$

where k_0 is the reaction constant, which can be determined experimentally.

iv. The post-leaching residue was found to be constituted of microline and quartz.

References

Ajemba, R. O., Onukwuli, O. D. (2012). Application of the shrinking core model to the analysis of alumina leaching from Ukpor clay using nitric acid. *International Journal of Engineering Research & Technology, 1*(3), 1-13.

Al – Sindy, S. I., Al – Ajeel, A., Wahab, A. (2006). Alumina Recovery from Iraqi kaolinitic clay by hydrochloric acid route. *Iraqi Bulletin of Geology and Mining, 2*(1), 67 – 76.

Aydogan, S., Erdemoglu, M., Ucar, G., Aras, A. (2007a). Kinetics of galena dissolution in nitric acid solutions with hydrogen peroxide. *Hydrometallurgy, 88*, 52-57.

Aydogan, S., Erdemoglu, M., Ucar, G., Aras, A. (2007b). Dissolution kinetics of galena in acetic acid solutions with hydrogen peroxide. *Hydrometallurgy, 89*,189-195.

Baba, A. A., Adekola, F. A. (2010). Hydrometallurgical Processing of a Nigerian Sphalerite in Hydrochloric Acid: Characterization and dissolution kinetics. *Hydrometallurgy, 101*, 69 – 75.

Brown, W. H., Hrishikesan, K. G. (1966). Process for the production of alumina. United States Patent Online, No. 3, 240, 562.

Connor, D. J. (1988). Alumina extraction from non-bauxiticmaterials:Aluminium. VerlagGmbh, Dusseldorf, 370.

Divacaran, R. and Sivasankara, V. N. (2004). Mechanism of kaolinite and titanium dioxide flocculation using chitosan-assistance by fulvic acids. *Water Res., 38*, 2135 - 2143.

Dutrizac, J. E., MacDonald, R. J. C. (1977). CIM Annual Volume, 186 – 194.

Fuerstenau, M. C., Chen, C. C., Han, K., Palmer, R. B. (1986). Kinetics of galena dissolution in ferric chloride solutions. *Metall. Mater. Trans. B*, 17, 415.

Habashi, F. (2005). Hydrometallurgy of lead. *Metallurgia, 59* (3), 114 -118.

Hutchison, C. S. (1974). Laboratory Handbook of Petrography Techniques, first ed., John Wiley and Sons Inc., New York, pp. 1-14.

Khalique, A., Akram, A., Ahmed, A. S., Hamid, N. (2005). Effect of sodium chloride on dissolution of galena in aqueous acid solution. *Pak. J. Sci. Ind. Res., 48* (4), 236 – 239.

Leao, V. A., Souza, A. D., Pina, P. S., Silva, C. A., Siqueira, P. F. (2007). The leaching kinetics of a zinc sulph-ide concentrate in acid ferric sulphate. *Hydrometallurgy, 89*; 72 – 81.

Merwe, W. (2003). Dissolution of sphalerite minerals from Rosh Pinah Tailings, Magister Scientiae, Faculty of Natural and Agric. Sciences, University of Pretoria, p. 106.

Olanipekun, E. O., Oderinde, R. A. (1999). Hydrochloric acid leaching of sphalerite in the presence of an oxidizing agent. *Park. J. Sci. Ind. Res. 42*(4), 204 – 208.

Raghavan, P., Chandrasekhar, S., Vogt, V., Gock, E. (2004). Separation of titanoferrous impurities from Kaolin by high shear pretreatment and froth flotation. *Appl. Clay Sci. 25*, 111-120.

Schroeder, P. A., Melear, N. D., Pruett, R. J. (2003). Quantitative analysis of anatine in Georgia kaolin using Raman spectroscopy. *Appl Clay Sci. 23*, 299 – 308.

Souza, A. D., Pina, P.S., Leao, V. A., Silva, C. A., Siqueira, P. F. (2007). The leaching kinetics of a zinc sulphide concentrate in acid ferric sulphate. *Hydrometallurgy*, 89, 72-81.

Sthay, C., Ramaswamy, S. (2002). Influence of mineral impurities on the properties of kaolin and its thermally treated products. *Appl. Clay Sci., 21*, 133 – 142.